Highly regenerative species-specific genes improve age-associated features in the adult *Drosophila* midgut

Hiroki Nagai[1], Junichiro Ui[1], Tenki Nakasugi[1], Takashi Makino[2], Masayuki Miura[1], and Yu-ichiro Nakajima[1] *

1. Graduate School of Pharmaceutical Sciences, The University of Tokyo

2. Graduate School of Life Science, Tohoku University

*Author for correspondence e-mail: nakaji97@g.ecc.u-tokyo.ac.jp

Tel: +81-3-5841-4863

Text: 29632 characters

Figures: 6

Supporting information: supplemental figures S1-S3, supplemental tables S1-S2, supplemental texts S1

Abstract

The remarkable regenerative abilities observed in planarians and cnidarians are closely linked to the active proliferation of adult stem cells and the precise differentiation of their progeny, both of which typically deteriorate during aging in low regenerative animals. While regeneration-specific genes conserved in highly regenerative organisms may confer regenerative abilities and long-term maintenance of tissue homeostasis, it remains unclear whether introducing these regenerative genes into low regenerative animals can improve their regeneration and aging processes. Here we ectopically express high regenerative species-specific JmjC domain-encoding genes (HRJDs) in *Drosophila*, a widely used low regenerative model organism. Surprisingly, HRJD expression impedes tissue regeneration in the developing wing disc but extends organismal lifespan when expressed in the intestinal stem cell lineages of the adult midgut under non-regenerative conditions. Notably, HRJDs enhance the proliferative activity of intestinal stem cells while maintaining their differentiation fidelity, ameliorating age-related decline in gut barrier functions. These findings together suggest that the introduction of highly regenerative species-specific genes can improve stem cell functions and promote a healthy lifespan when expressed in aging animals.

Keywords

Synthetic biology, aging, healthy lifespan, regeneration, *Drosophila*, intestinal stem cells

INTRODUCTION

Regeneration, an intricate process that rebuilds lost body parts, is a widespread phenomenon among metazoans, but the capacity for regeneration displays significant variation across different groups and species [1–5]. While certain animals like planarians and hydras possess the remarkable ability to regenerate their entire body from a small fragment, other groups with more complex body structures, such as mammals and insects, exhibit a diminished regenerative potential and can only regenerate specific tissues and/or organs to a limited extent. Furthermore, regenerative capacity often declines with aging in most species with limited regeneration abilities [2], resulting in increased susceptibility to organismal death upon injury. In contrast, animals that can achieve whole body regeneration, along with developmental reversion observed in the jellyfish *Turritopsis*, exhibit potential immortality [2, 5, 6]. Understanding the mechanisms underlying high regenerative ability and their relationship with aging represents a fundamental challenge in the field of developmental biology and gerontology with implications for regenerative medicine.

Several cellular and molecular factors have been identified as determinants of regeneration capacity. Highly regenerative animals such as planarians and cnidarian polyps rely on pluripotent adult stem cells, called neoblasts and interstitial cells (i-cells), respectively [2–5, 7]. These stem cells migrate to the injury sites and contribute to the formation of a blastema, an undifferentiated cellular mass, enabling the restoration of amputated body structures. Some vertebrates like salamanders and fish, which do not possess adult pluripotent stem cells, can regenerate organs after injury by recruiting

64 blastema cells through dedifferentiation and/or the activation of quiescent lineage-
65 restricted stem cells [1, 2, 4, 5, 8]. At the molecular level, the evolutionary conserved
66 WNT signaling pathway promotes a wide range of regenerative events across species,
67 including blastema formation in newts and *Hydra* [1–5, 8].

68 In contrast to the conserved regulators of regeneration, several genes are
69 specific to highly regenerative animal groups and species: for instance, the newt gene
70 *Prod1* regulates re-patterning during limb regeneration [9, 10], and viropana family
71 (*viropana 1-5*) is up-regulated during lens regeneration [11, 12]. These species/group-
72 specific genes might explain differences in regeneration capacity between species.
73 Remarkably, ectopic expression of *viropana 1-5* can enhance regeneration of the
74 primordium of *Drosophila* eyes that maintain regenerative capacity during development
75 [12]. This finding raises the possibility that heterologous induction of regenerative genes
76 may accelerate tissue regeneration, at least in developing animals, and potentially provide
77 a cue for developing novel regenerative therapies. However, it remains unknown whether
78 heterologously-induced regenerative genes can improve regenerative and/or aging
79 processes even when induced in post-developmental mature adults.

80 Notably, given that basal metazoans such as Porifera, Ctenophore, Placozoa,
81 and Cnidaria all exhibit robust regenerative abilities, it is conceivable that a common
82 ancestor of all metazoans once possessed a high regenerative potential and independently
83 lost genes related to high regenerative capacity in multiple phyla. Building upon this
84 hypothesis, bioinformatics analysis has identified genes that are common among species
85 with high regenerative abilities and absent in species with limited regenerative capacities

86 (Fig. 1A) [13]. The highly regenerative species-specific JmjC domain-encoding genes
87 (HRJDs) are a group of such genes characterized by their JmjC domain (Fig. 1A), yet
88 their molecular functions remain unknown. Given their potential influence on the
89 regenerative process, HRJDs may contribute to the high regeneration potential of highly
90 regenerative animals. With this in mind, a question arises: what would happen if a low
91 regenerative species, which has lost HRJDs, were to acquire them again? By ectopically
92 expressing HRJDs in low regenerative animal models, we can investigate their impacts
93 on regeneration as well as on aging processes, providing insight into the role of HRJDs.
94 Here we express HRJDs in the fruit fly *Drosophila melanogaster* and evaluate
95 their impact *in vivo*, especially by focusing on two epithelial tissues: developing wing
96 discs and post-developmental adult midguts, both of which exhibit regeneration potential
97 and can replenish damaged epithelial cells. In contrast to the predicted contribution of
98 HRJDs in regeneration as observed in planarian, ectopic HRJD induction impedes
99 regenerative responses and decreases organismal survival upon injury in *Drosophila*.
100 Surprisingly, however, HRJD expression in the stem/progenitor population of the adult
101 midguts extends organismal lifespan under the non-regenerative condition. Further
102 investigations reveal that HRJDs enhance the proliferative activity of intestinal stem cells
103 while keeping their differentiation fidelity in aged guts, ameliorating age-related decline
104 in gut barrier functions. These findings provide evidence that genes specific to highly-
105 regenerative animals can improve stem cell function as well as increase healthy lifespan
106 upon heterologous expression in aging animals.
107

108 **RESULTS**

109 **Planarian HRJDs expression do not affect gross morphology of fly adults**

110 Planarians are one of the most highly regenerative animals; they are capable of
111 regenerating most body parts upon amputation and can even reconstruct their whole
112 body from fragments [1–4, 8, 14]. Previous work has identified two HRJD orthologs
113 *HRJDa* and *HRJDb* from two planarian species, *Dugesia japonica* and *Schmidtea*
114 *mediterranea* (Fig. 1B) [13]. In functional assays using RNAi-mediated knockdown in
115 *D. japonica*, these two HRJDs affect viability of organisms after amputation [13],
116 suggesting that planarian HRJDs are associated with regeneration processes. We thus
117 utilized these functional HRJDs in *D. japonica* as representatives for the following
118 studies and hereafter simply named them as HRJDa and HRJDb.

119 To examine potential benefits and/or disadvantages of acquiring HRJDs, we
120 then ectopically expressed HRJDs in *Drosophila melanogaster*, which has lost HRJD
121 genes during evolution (Fig. 1A), using the Gal4/UAS system (Fig. S1) [15]. We first
122 introduced HRJDs in the whole body throughout development with the ubiquitous driver
123 *Act5C-Gal4* (Fig. 1C, *Act5C-Gal4>UAS-HRJDa/b*). The whole body expression of
124 HRJDs neither caused developmental lethality nor changed the body weight of mature
125 adults compared with the *Act5C-Gal4>UAS-GFP* control (Fig. 1D and 1E). We further
126 assessed the gross morphology of adult wings and eyes under the ubiquitous expression
127 of HRJDs. The wing size was not altered by HRJD expression (Fig. 1F and 1G). Similarly,
128 *Act5C-Gal4>UAS-HRJDa/b* flies did not change the size of adult compound eyes (Fig.
129 1H and 1I). These results indicate that HRJD expression does not disturb gross

130 morphology of adult flies under homeostatic conditions, likely due to minimal impacts
131 on developmental processes.
132
133 **HRJD expression hampers tissue regeneration in the developing wing disc**
134 Given that HRJDs are conserved only among highly regenerative animals, their primary
135 functions may be related to regeneration processes. Indeed, both planarian HRJDa and
136 HRJDb function in whole-body regeneration while their relative contribution is likely
137 context-dependent: HRJDa is indispensable for the regeneration of amputated heads
138 while HRJDb promotes organismal survival after two consecutive amputations [13]. To
139 test whether heterologously-induced HRJDs can enhance regenerative responses in
140 *Drosophila*, we examined their impacts on regeneration after ablation of the developing
141 wing imaginal disc. The *Drosophila* larval imaginal discs, including wing discs, which
142 are composed of columnar epithelial cells, exhibit regenerative capacity and restore
143 morphology even after massive cell death [16, 17] (Fig. 2A and 2B). We utilized the
144 genetic ablation system in which transient overexpression of *eiger*, a *Drosophil*a TNF
145 ligand, induces apoptosis in the wing pouch region [17, 18]. In this tissue ablation system,
146 the temperature-sensitive form of the Gal4 repressor Gal80 (*tub-Gal80*^{ts}) allows transient
147 tissue ablation under the control of a wing pouch driver *rn-Gal4.* To circumvent the
148 temporal expression associated with the Gal4/Gal80^{ts} system, we further introduced an
149 additional binary expression system: the QF/QUAS system for HRJD induction (Fig. 2A)
150 [19, 20]. When expressing HRJDs in the wing pouch with the *WP-QF* driver during the
151 entire process of recovery, we found that *WP-QF>QUAS-HRJDs* flies exhibit severe

152 defects compared to controls (Fig. 2C). Importantly, HRJD induction in the wing disc did
153 not affect the development of adult wing under homeostatic condition (Fig. 2D and 2E).
154 These results suggest that HRJD expression does not facilitate regeneration in the
155 developing wing disc epithelium.
156
157 **HRJD expression compromises regeneration in the adult midgut**
158 Most highly regenerative animals exhibit regeneration potential in mature adult stages
159 [2–4, 8], and thus one possibility is that HRJDs stimulate regenerative responses only in
160 adults, where tissue-resident stem cells play an important role in homeostasis and
161 regeneration. We thus tested the impact of HRJD expression on the regenerative capacity
162 of the *Drosophila* adult midgut. In the adult midgut, intestinal stem cells (ISCs) self-
163 renew ISCs themselves and also generate differentiating progenitor cells called
164 enteroblasts (EBs) and enteroendocrine progenitors (EEPs), which eventually
165 differentiate into absorptive enterocytes (ECs) and secretory enteroendocrine cells (EEs),
166 respectively (Fig. 3A) [21–24]. The adult midgut activates proliferation of ISCs in
167 response to orally-treated harmful chemicals such as paraquat and dextran sulfate sodium
168 (DSS), a regenerative response that is essential for organismal survival [21, 25–28]. We
169 thus expressed HRJDs in ISCs and EBs using the *esg-Gal4* (*esg-Gal4>UAS-HRJDa/b*)
170 driver and tested survival against paraquat/DSS damage. Similar to the wing regeneration
171 assay, continuous expression of HRJDs via *esg-Gal4* significantly impaired organismal
172 survival upon the chemical challenges, with a stronger effect for HRJDa (Fig. S2A and
173 S2B). Survival under control feeding (5% sucrose) was also slightly decreased by HRJD

174 expression, albeit not to a statistically significant degree (Fig. S2C). We further examined
175 ISC proliferation after paraquat feeding by counting the number of cells marked with a
176 mitotic marker, anti-phospho histone H3 (PH3) staining, and found that induction of
177 HRJDa significantly suppressed ISC division (Fig. S2D), which is consistent with the
178 stronger decline in survival rate. Concordant with the wing ablation experiments, these
179 results suggest that continuous HRJD expression causes detrimental effects to
180 regenerative capacity.

181 Because the *esg-Gal4* driver is active not only in adult ISCs/EBs but also in the
182 proliferative adult midgut progenitors in the larval midguts and larval imaginal discs [29,
183 30], continuous HRJD expression may cause internal organ defects associated with
184 development. To temporally restrict HRJD expression to the adult stage, we next set up
185 an experiment where HRJD expression starts only in adults after eclosion from pupa by
186 combining *esg-Gal4* with *tub-Gal80*^{ts} (*esg-Gal4*^{ts}*>UAS-HRJDa/b*) (Fig. 3B); however,
187 neither HRJDa nor HRJDb improved organismal survival upon paraquat/DSS feeding
188 (Fig. 3C and 3D). Instead, HRJDa expression caused a slight but significant decrease in
189 survival rate compared with control (*esg-Gal4*^{ts}*>UAS-GFP*) (Fig. 3C and 3D). Survival
190 under control feeding (5% sucrose) was comparable between *esg-Gal4*^{ts}*>UAS-GFP* and
191 *esg-Gal4*^{ts}*>UAS-HRJDa/b* (Fig. 3E), suggesting that the impaired survival of *esg-*
192 *Gal4*^{ts}*>UAS-HRJDa* is specific to regenerative contexts. We also confirmed that there
193 were no significant changes in mitotic cell numbers in HRJD expressing flies compared
194 to controls (Fig. 3F and 3G). These results indicate that post-developmental expression
195 of HRJDs does not enhance intestinal regeneration in adult flies.

196

197 **Post-developmental HRJD expression in ISC lineages extends organismal lifespan**

198 Highly-regenerative animals are often resistant to organismal aging and have long
199 lifespan; some species like the jellyfish *Turritopsis* even revert their early developmental
200 stages under harsh environments and are considered to be potentially immortal [2, 6].
201 Although heterologous expression of HRJDs does not augment tissue regeneration in
202 either developing or adult *Drosophila* tissues, we further investigated whether HRJDs
203 influence organismal lifespan under homeostatic conditions in which no experimental
204 injuries are applied to fly adults. We observed that post-developmental HRJD expression
205 in adult ISCs/EBs (*esg-Gal4*^{ts}*>UAS-HRJDa/b*) significantly extended organismal
206 lifespan both in females (Fig. 4A) and males (Fig. 4B). In contrast, continuous HRJD
207 expression in the whole body (*Act5C-Gal4>UAS-HRJDa/b*) shortened males' lifespan
208 (Fig. 4C and 4D). Moreover, HRJD expression in differentiated ECs (*NP1-Gal4>UAS-*
209 *HRJDa/b*) also negatively impacted female lifespan, likely due to developmental
210 abnormalities since EC-specific HRJD expression in the adult stage did not affect survival
211 (Fig. S3A-S3D). These results suggest that spatio-temporally regulated induction of
212 HRJDs in adult ISCs/EBs can be beneficial for adult flies under homeostatic conditions.

213 Further investigation revealed the distinct impacts of HRJDa and HRJDb on
214 organismal lifespan: while continuous expression of HRJDa via *esg-Gal4 (esg-*
215 *Gal4>UAS-HRJDa)* shortened lifespans for both males and females, *esg-Gal4>UAS-*
216 *HRJDb* prolonged female lifespans but shortened male lifespans (Fig. S3E and S3F). The
217 ortholog-dependent phenotypic differences were also reported in planarian regeneration

218 [13]. To address the mechanisms of lifespan extension associated with post-
219 developmental HRJD expression in ISCs/EBs, we focused on *esg-Gal4^{ts}>UAS-HRJDs*
220 midguts in the following experiments.
221
222 **HRJD expression attenuates mis-differentiation of stem cell lineage in the aged**
223 **intestine**
224 Age-related mortality accompanies intestinal barrier dysfunction and disruption of cell-
225 cell junction in the gut epithelium across species [31–34]. Given that aging phenotypes
226 are more severe in female flies than male flies [35], we first tested barrier function of the
227 *esg-Gal4^{ts}>UAS-HRJDa/b* female midgut using the Smurf assay, in which orally-
228 administered blue dye spreads throughout the entire body when the intestinal barrier is
229 disrupted (Smurf+, Fig. 5A) [31, 35]. Consistent with lifespan extension, post-
230 developmental HRJD expression in ISCs/EBs significantly decreased the ratio of Smurf+
231 adults at 30-days old, a time point where age-related organismal death starts (Fig. 4A and
232 5A), suggesting that barrier function is maintained in aged flies that express HRJDs in
233 ISCs/EBs. We further assessed the localization of septate junction markers (Dlg, Tsp2A,
234 Mesh, Ssk), which diffuse in cytoplasm in the aged midgut [33, 36–38]. The diffusion of
235 the Dlg protein in aged midguts was significantly suppressed in *esg-Gal4^{ts}>UAS-*
236 *HRJDa/b* midguts (Fig. 5B and 5C). Similarly, peripheral localization of Tsp2A, Mesh,
237 and Ssk proteins was also maintained in *esg-Gal4^{ts}>UAS-HRJDa/b* midguts compared
238 with control (*esg-Gal4^{ts}>UAS-GFP*) midguts (Fig. 5D-5I). These results indicate that

239 HRJD expression in adult ISCs/EBs contributes to the prolonged maintenance of the
240 junctional integrity as well as gut barrier function in the aged intestine.

241 In addition to the intestinal barrier dysfunction, aberrant activation of ISC
242 mitosis and accumulation of mis-differentiated ISC progenies are also common age-
243 related phenotypes in the *Drosophila* adult midgut [27, 31, 33, 39]. In 30-days old control
244 midguts, *esg-Gal4*^{ts}*>UAS-GFP*$^{+}$ cells exhibited hallmarks of age-related mis-
245 differentiation into enterocytes such as increased ploidy and enlarged nuclear size (Fig.
246 6A) [27]. By contrast, we found that HRJD expression in adult ISCs/EBs suppressed these
247 mis-differentiation phenotypes (Fig. 6A and 6B), which are consistent with the
248 amelioration of age-related barrier dysfunction in *esg-Gal4*^{ts}*>UAS-HRJDa/b* midguts.
249 Surprisingly, however, *esg-Gal4*^{ts}*>UAS-HRJDa/b* did not suppress age-related increase
250 in ISC proliferation, but rather enhanced it in 30-day old midguts (Fig. 6C and 6D). The
251 enhancement of ISC proliferation was specific to the aged intestine since *esg-*
252 *Gal4*^{ts}*>UAS-HRJDs* did not affect PH3^{+} cell number in 10-day-old young midguts (Fig.
253 6D). These results raised the possibility that HRJD expression augments the mitotic
254 activity of stem cells while maintaining their differentiation fidelity during aging. To test
255 this hypothesis, we measured the expression of cell type markers (*Delta* for ISCs, *nub* for
256 enterocytes, and *pros* for enteroendocrine cells) by RT-qPCR of whole midguts. Both *nub*
257 and *pros* are negatively regulated by Esg [40, 41], and accumulation of *esg*$^{+}$ mis-
258 differentiated cells accompanies the down-regulation of EC-related genes in aged midguts
259 [27]. Consistent with enhanced ISC proliferation, *esg-Gal4*^{ts}*>UAS-HRJDa* significantly
260 up-regulated *Delta* expression in 30-day old midguts (Fig. 6E). More importantly, *esg-*

261 *Gal4^{ts}>UAS-HRJDa* also up-regulated *nub* and *pros*, which supports our hypothesis that
262 HRJDs improve proper differentiation of ISC progenies. On the other hand, *esg-*
263 *Gal4^{ts}>UAS-HRJDb* mildly increased *Delta* expression, although *nub* and *pros* were not
264 significantly up-regulated (Fig. 6E). Taken together, our results show that post-
265 developmental expression of HRJDs improves stem cell functions in aged intestine, while
266 the underlying mechanisms between HRJDa and HRJDb likely differ.
267

268 **DISCUSSION**

269 In this study, we demonstrate that post-developmental expression of planarian HRJD
270 genes in the *Drosophila* adult ISCs/EBs can suppress age-related intestinal dysfunctions
271 and extend organismal lifespan, while their continuous expression throughout the entire
272 developmental process hampers regenerative responses and principally shortens lifespan.
273 Notably, HRJDs in adult ISCs/EBs boost the age-related increase of ISC proliferation but
274 do not cause age-related mis-differentiation of ISC progenies (Fig. 6F). These HRJD-
275 mediated outcomes are distinct from those mediated by typical anti-aging manipulations
276 such as antibiotic treatment and metabolic intervention, which ameliorate both ISC over-
277 proliferation and mis-differentiation [24, 31, 42]. Therefore, heterologously induced
278 HRJDs create the neomorphic state in the aged intestine (Fig. 6F). Given the age-related
279 increase of chronic cellular stresses [24, 27, 36, 42, 43], we speculate that the HRJD-
280 dependent ISC activation and their proper differentiation improve organismal fitness by
281 enabling active turnover of damaged intestinal cells.

282 The typical JmjC family proteins function as histone demethylase or nucleic
283 acid/protein hydroxylase. Domains other than the JmjC domain determine which
284 enzymatic functions are exerted; for instance, the tudor domain and PHD domain confer
285 demethylase activity [44]. However, HRJDs contain only the JmjC domain and the EF
286 hand motif (Fig. 1B), which makes it difficult to address the molecular functions of
287 HRJDs. Among the JmjC-domain containing genes, HRJDs have been predicted to be
288 closest to KDM8 [13], and human KDM8 activates cancer cell proliferation via
289 demethylation of H3K36me2 on the cyclin A1 locus [45]. These reports imply the
290 possibility that HRJDs function as histone demethylase like KDM8. If this is the case,
291 HRJDs must access chromatins; however, we found that ectopically-induced HRJDs
292 localize in the cytoplasm but not in the nucleus both *in vitro* (S2 cells) and *in vivo* (wing
293 discs and adult midguts) (Fig. S1B-S1D), which is a common localization pattern of
294 JmjC-domain only proteins [46, 47]. Interestingly, *Drosophila* JmjC-domain only genes
295 such as *JMJD4/5/7* genetically interact with loss of function of *snr1*, a component of the
296 SWI/SNF complex [48], and the mammalian ortholog of *snr1*, SMARCB1, binds to
297 mitotic chromatin to ensure proliferating activity of daughter cells [49]. It is thus tempting
298 to speculate that HRJDs may access chromatins during mitosis, when nuclear membrane
299 disappears, to regulate stem cell functions in the *Drosophila* adult midgut.

300 Although HRJDs have been identified as genes conserved between highly
301 regenerative animals [13], it is unclear whether HRJDs alone are sufficient to enhance
302 regenerative responses. Our investigations revealed that ectopic expression of HRJDs
303 failed to improve regeneration of developing wing discs and adult midguts in *Drosophila*

304 (Fig. 2 and 3). However, it should be noted that we induced HRJDs before tissue injury
305 and maintained their expression during regeneration period. Given that *HRJDb* is up-
306 regulated in the late phase of planarian regeneration (3 days after amputation) [13], strict
307 regulation of HRJD induction might be important for their proper function as true
308 regeneration regulators. On the other hand, the expression level of *HRJDa* remains
309 constant during planarian regeneration [13], which is recapitulated in our experiments.
310 Another possibility is that a high regeneration ability can be achieved by cooperation
311 between HRJDs and other unidentified genes that have been lost during evolution, which
312 should be addressed in future studies.

313 During the normal aging process in the *Drosophila* adult midgut, ISC over-
314 proliferation is closely linked with other aging phenotypes, and suppression of ISC
315 division can prevent the accumulation of mis-differentiated ISC progenies and extend
316 organismal lifespan [24, 36, 42, 43]. In contrast, HRJDs enhance age-related ISC
317 activation but can alleviate mis-differentiation and extend lifespan, suggesting that it is
318 not ISC activation itself but rather mis-differentiation of ISC progenies that principally
319 drives age-related mortality. Consistently, manipulation of mitotic spindle orientation,
320 which affects the cell fate of daughter cells [50–52], can extend organismal lifespan
321 without changing mitotic activity of ISCs [52]. Of note, in contrast to *Drosophila* ISCs
322 which over-proliferate in aged midguts, many adult stem cells decrease their activity and
323 abundance during aging both in *Drosophila* and mammals [24, 53, 54]. Future
324 investigations for mechanisms of HRJD-mediated stem cell rejuvenation will provide
325 clues to develop new anti-aging strategies.

326

Methods

Drosophila stocks

All stocks were maintained on a standard diet containing 4% cornmeal, 6% baker's yeast (Saf Yeast), 6% glucose (Wako, 049-31177), and 0.8% agar (Kishida chemical, 260-01705) with 0.3% propionic acid (Tokyo Chemical Industry, P0500) and 0.05% nipagin (Wako, 132-02635). Canton S was utilized as the wildtype strain. Transgenic fly lines were obtained from the Bloomington Drosophila Stock Center (BDSC) and the Kyoto Stock Center: *Act5C-Gal4* (BDSC 3954), *rn-Gal4, tub-Gal80ts, UAS-egr* (BDSC 51280), *WP-QF2* (Kashio 2016) [55], *tub-Gal80ts* (BDSC 7017, 7019), *esg-Gal4* (Kyoto 109126), *NP1-Gal4* (Kyoto 112001), *UAS-GFP* (BDSC 1522), M{3xP3-RFP.attP}ZH-86Fb (Kyoto 130437), UAS-HRJDa (this study), UAS-HRJDb (this study), QUAS-HRJDa (this study), QUAS-HRJDb (this study), UAS-FLAG-HRJDa (this study), UAS-FLAG-HRJDb (this study). See **Table S1** for genotypes in each Figure. We used female flies unless otherwise noted in the Figures.

Drosophila genetics

Experimental crosses that did not involve Gal80^{ts}-mediated inhibition of Gal4 were performed at 25°C. When using Gal80ts, experimental crosses were maintained at 18°C, and F1 adults were transferred to 29°C three days after eclosion. Midgut staining and Smurf assays were performed after 7 or 27 days of 29°C incubation (young: Day 10 adults, old: Day 30 adults).

Generation of HRJD expressing lines

To express HRJDs using the Gal4/UAS or the QF/QUAS system, we constructed a vector containing *HRJDa* or *HRJDb* under the control of either the UAS sequence or QUAS sequence. Namely we amplified HRJDa and HRJDb sequence from codon-optimized synthesized DNAs (pUCIDT-HRJDa and pUCIDT-HRJDb, IDT, Supplementary texts S1) for *DjHRJDa* and *DjHRJDb*, respectively. UAS-HRJDa and UAS-HRJDb were constructed by ligating HRJDa and HRJDb into pUAST-attB (DGRC 1419), respectively (digested by EcoRI/NotI). Similarly, QUAS-HRJDa and QUAS-HRJDb were constructed by ligating HRJDa and HRJDb into pQUAS-WALIUM20 (DGRC 1474), respectively

359 (digested by NheI/EcoRI). To construct UAS-3xFLAG-HRJDs, we PCR-amplified the
360 coding sequences of HRJDs from pUCIDT-HRJDs by gene-specific primers with
361 3xFLAG tag at 5'-end of the forward primers, and the amplicons were then ligated into a
362 pUAST-attB vector digested by EcoRI/NotI using In-Fusion HD Cloning Kit (Takara,
363 639649). The landing site for each construct was {3xP3-RFP.attP}ZH-86Fb. Injection
364 and selection were performed by WellGenetics (Taiwan, R.O.C.). Please see also Table
365 S2 and Supplementary texts S1 for primer sequences and HRJDs sequences.
366
367 **S2 cell culture**
368 *Drosophila* S2 cells were grown at 25°C in Schneider's *Drosophila* medium (GIBCO,
369 21720001) supplemented with 10% (v/v) heat-inactivated fetal bovine serum (FBS), 100
370 U/mL penicillin, and 100 μg/mL streptomycin (FUJIFILM Wako, 168–23191).
371
372 **S2 cell immunostaining**
373 To examine the expression pattern of HRJDs through immunostaining, 1×10^6 cells were
374 seeded in 6-well plates containing Schneider's *Drosophila* medium supplemented with
375 10% (v/v) heat-inactivated fetal bovine serum, 100 U/mL penicillin, and 100 μg/mL
376 streptomycin and were transfected with 800 ng of pAc5-3xFLAG-HRJDs using Effectene
377 Transfection Reagent (QIAGEN, 301427) following the manufacturer's protocol. To
378 prepare pAc5-3xFLAG-HRJDs, we amplified the coding sequences of HRJDs from
379 pUCIDT-HRJDs (Supplementary texts S1) by gene-specific primers with 3xFLAG tag at
380 5'-end of the forward primers, and the amplicons were then ligated into a pAc5-
381 STABLE2-neo (Addgene, 32426) [56] digested with EcoRI/XhoI by In-Fusion HD
382 Cloning Kit (Takara, 639649). Twenty-four hours after transfection, the cells were
383 washed with PBS and the medium was replaced with fresh Schneider's *Drosophila*
384 medium supplemented with 10% (v/v) heat-inactivated FBS, 100 U/mL penicillin, and
385 100 μg/mL streptomycin. Forty-eight hours after transfection, the cells were fixed with
386 4% paraformaldehyde (PFA) in PBS, washed with PBS containing 0.1% Triton X-100
387 (PBST), blocked in PBST with 5% normal donkey serum (PBSTn), and incubated with
388 primary antibodies in PBSTn overnight at 4 °C. The samples were then washed with
389 PBST, incubated for 1 h at room temperature with secondary antibodies and Hoechst
390 33342 suspended in PBSTn and washed again with PBST. Images were captured using
391 an LSM880 with Airyscan (Zeiss). The primary antibody used was a mouse anti-FLAG

392 M2 monoclonal antibody (1 : 2000, Sigma, F1804). The secondary antibodies used were
393 Goat anti-Mouse IgG2b Cross-Adsorbed Secondary Antibody, Alexa Fluor™ 555
394 (1:2000, Thermo Fisher Scientific, A-21147). Hoechst 33342 (0.4 μM; Invitrogen,
395 H3570) was used for nuclear staining. Images were analyzed and edited using Fiji/ImageJ
396 software (NIH).
397
398 **S2 cell western blotting**
399 To examine the expression of HRJDs, 2.5 × 10^5 cells were seeded in 24-well plates
400 containing Schneider's *Drosophila* medium supplemented with 10% (v/v) heat-
401 inactivated FBS, 100 U/mL penicillin, and 100 μg/mL streptomycin and were transfected
402 with 200 ng of pAc5-3xFLAG-HRJDs using Effectene Transfection Reagent (QIAGEN,
403 301427) following the manufacturer's protocol. Twenty-four hours after transfection, the
404 cells were washed with PBS and the medium was replaced with fresh Schneider's
405 *Drosophila* medium supplemented with 10% (v/v) heat-inactivated FBS, 100 U/mL
406 penicillin, and 100 μg/mL streptomycin. Forty-eight hours after transfection, the cells
407 were washed with PBS and lysed with 50 μL RIPA buffer supplemented with cOmplete
408 ULTRA EDTA-free protease inhibitor cocktail (Roche, 05892953001). The lysate was
409 sonicated and centrifuged at 20,000 g for 5 minutes. Protein concentration was
410 determined by BCA assay. The supernatant was mixed with SDS, boiled at 95 °C for 5
411 minutes, and subjected to western blotting.
412 Proteins were separated using SDS-PAGE and transferred onto Immobilon-P
413 PVDF membranes (Millipore, IPVH00010) for immunoblotting. Membranes were
414 blocked with 4% skimmed milk diluted in 1×Tris buffered saline containing 0.1% Tween-
415 20. Immunoblotting was performed using the below-mentioned antibodies, which were
416 diluted with 4% skim milk. The signals were visualized using Immobilon Western
417 Chemiluminescent HRP Substrate (Millipore, WBKLS0500) and FUSION SOLO. 7S.
418 EDGE (Vilber-Lourmat). Contrast and brightness adjustments were applied using the
419 Fiji/ImageJ software (NIH).
420 The primary antibody used was mouse anti-FLAG M2 monoclonal antibody
421 (1 : 5000, Sigma, F1804). Mouse anti-alpha tubulin (DM1A) monoclonal antibody
422 (1 : 5000, Sigma, T9026) was used as loading control. The secondary antibody used was
423 HRP-conjugated goat/rabbit/donkey anti-mouse IgG (1 : 10000, Promega, W402B).
424

425 **Drug treatment**
426 5 mM paraquat (Sigma, 856177) and 5% (w/v) DSS (MP Biomedicals, 160110) were
427 dissolved in 5% (w/v) sucrose solution. Filter paper (Whatman 3MM) was soaked with
428 400 µl of these reagents and placed into empty vials. For histological analyses, flies were
429 fed with the reagent solution for 1 day. For the survival assay, flies were transferred to
430 new vials and dead flies (determined by immobility and showing no response to tapping)
431 were counted every day. 5% sucrose was used for control feeding.
432
433 **Immunofluorescence**
434 Samples were dissected in 1X PBS and fixed in 4% PFA for 20 minutes (wing discs) and
435 30-45 minutes (adult midgut) at room temperature (RT), respectively. The following
436 primary antibodies were used with indicated dilution into 1X PBS containing 0.5% BSA
437 and 0.1% Triton X-100: rabbit anti-PH3 (Millipore 06-570, 1:1000), mouse anti-FLAG
438 (Sigma F1804, 1:1000), mouse anti-Dlg (DSHB 4F3, 1:100), rabbit anti-GFP (MBL 598,
439 1:500), rat anti-GFP (Nacalai tesque 04404-26, 1:400), rabbit anti-Tsp2A (Izumi et al.,
440 2016, 1:1000) [57], rabbit anti-Mesh (Izumi et al., 2012, 1:1000) [58], rabbit anti-Ssk
441 (Izumi et al., 2016, 1:1000) [57]. After overnight incubation with primary antibodies at
442 4°C, samples were incubated with fluorescent secondary antibodies (Jackson
443 ImmunoResearch and Invitrogen, 1:500) for 1 hour at RT. Hoechst 33342 (Invitrogen,
444 final concentration: 10 µg/ml) was used to visualize DNA. Wing discs were mounted as
445 described previously [59, 60]. Samples were mounted in Slowfade Diamond
446 (ThermoFisher, S36963) and imaged with confocal microscopy (Zeiss LSM880).
447
448 **Smurf assay**
449 We referred to Rera et al. (2012) for the Smurf assay conditions [35]. To prepare the
450 feeding medium, 100 µl of 50% (w/v) brilliant blue FCF (Wako, 027-12842, final 2.5%)
451 and 100 µl of 5% (w/v) sucrose were added to a vial containing 2 ml of cornmeal-agar
452 food. After mixing with a spatula, an Whatman 1 filter (1001-020) was put on the feeding
453 medium. Flies were fed with this medium at 25°C for one day, after which they were
454 transferred to a new vial containing cornmeal-agar food without blue dye to clean the
455 epidermis. Two hours after the transfer, Smurf phenotype was checked. We classified the
456 Smurf phenotype as blue dye leakage outside abdomen (thorax, head, legs).
457

458 **Phylogenetic tree**

459 We created the phylogenetic tree of representative organisms using the NCBI taxonomy
460 browser (https://www.ncbi.nlm.nih.gov/Taxonomy/CommonTree/wwwcmt.cgi). The
461 species examined are *Amphimedon queenslandica* (Porifera), *Mnemiopsis leidyi*
462 (Ctenophora), *Trichoplax adhaerens* (Placozoa), *Hydra vulgaris* (Cnidaria), *Ptychodera*
463 *flava* (Hemichordata), *Acanthaster planci* (Echinodermata), *Branchiostoma floridae*
464 (Cephalochordata), *Ciona intestinalis* (Tunicata), *Danio rerio* (Teleostei), *Homo sapiens*,
465 *Mus musculus* (Mammalia), *Schmidtea mediterranea* (Platyhelminthes), *Caenorhabditis*
466 *elegans* (Nematoda), and *Drosophila melanogaster* (Arthropoda). These species, except
467 for *D. rerio, H. sapiens, M. musculus, C. elegans,* and *D. melanogaster,* are known to
468 have HRJDs and exhibit high regeneration ability [13]. The pictures were downloaded
469 from PhyloPic, and the color of some were changed from black to blue. Credits: Bennet
470 McComish (*B. floridae*), Malio Kodis (*M. leidyi*), and Markus A. Grohme (*S.*
471 *mediterranea*, https://www.phylopic.org/images/93f9611c-0cbd-4a14-92da-
472 004a4521e21f/schmidtea-mediterranea).
473

474 **Quantification of junctional proteins**

475 To quantify junctional and cytoplasmic intensity, a line that was orthogonal to one side
476 of a cell was drawn, and then the plot profile was calculated for the line. We defined the
477 junctional intensity as the highest value in that prolife, and defined cytoplasmic intensity
478 as the value 20 pixels (~2.6 μm) away from the highest value. Three lines were drawn for
479 one cell and the average of the three was used to represent the junctional/cytoplasmic
480 ratio for the cell. Six polyploid cells were randomly selected from each image for
481 quantification.
482

483 **Quantification of nuclear size**

484 Nuclei of *esg-Gal4>UAS-GFP* positive cells were traced by polygon selection tool and
485 added as ROI in Fiji/ImageJ. The size of each ROI was quantified using the Measure
486 command in Fiji/ImageJ.
487

488 **Statistics**

489 Statistical analyses were performed using Excel and RStudio. Two tailed *t* tests were used
490 for comparisons between two groups. One-way ANOVAs with post hoc Tukey tests were

performed when comparing three or more groups. Log-rank tests were used for comparison of survival curve. Significance is indicated in the Fig.s as follows: *P≤0.05, **P≤0.01, ***P≤0.001, Not Significant (N.S.): P>0.05. Bar graphs show mean ± standard error. Boxplots show median (thick line in the box), first and third quartiles (bottom and top of the box), minimum value (lower whisker), and maximum value (upper whisker). Dots in bar graphs and boxplots indicate individual values. Violin plots portray the distribution of individual values.

DECLARATIONS

Ethics approval and consent to participate

Not applicable.

Consent for publication

Not applicable.

Availability of data and materials

The datasets and *Drosophila* stocks used and/or analysed during the current study are available from the corresponding author on reasonable request.

Competing interests

The authors declare that they have no competing interests.

Funding

This work was supported by JSPS/MEXT KAKENHI (grant numbers JP22J01430 to H.N., JP21H04774, JP21K19206 to M.M., and JP17H06332, JP19K22550, JP22H02762 to Y.N.), AMED-Aging (JP21gm5010001 to M.M.), AMED-PRIME (JP22gm6110025 to Y.N.), and Sadako O. Hirai Ban Award for Young Researchers (H.N.)

Author contributions

Conceptualization: H.N., Y.N.

Investigation: H.N., J.U., T.N., Y.N.

Methodology: H.N., Y.N.

Validation: H.N., J.U., T.N., T.M., M.M., Y.N.

Data curation: H.N., T.M., Y.N.

Writing – original draft: H.N., J.U., T.M., Y.N.

Writing – review & editing: H.N., J.U., T.N., T.M., M.M., Y.N.

Supervision: M.M., Y.N.

Funding acquisition: H.N., T.M., M.M., Y.N.

Acknowledgements

We thank N. Shinoda, M. Furuse, Y. Izumi, BDSC, Kyoto Stock Center, Transgenic RNAi Project (TRiP), and DSHB for fly stocks and reagents.

536 **FIGURE LEGENDS**

537 **Figure 1. HRJD expression in whole body does not affect gross morphology.**

538 (A) Phylogenetic tree of HRJD conservation. Green indicates species that possess HRJD
539 gene(s) and gray indicates species that have lost HRJD gene(s). High regenerative ability
540 indicates that the species can regenerate their whole body or anterior/posterior body parts,
541 and low regenerative ability indicates that the species can only regenerate their appendage
542 (limbs, tails, fins) or much smaller scale of tissues/organs. We referred to Cao et al., 2019
543 for the definition of regenerative ability [13].

544 (B) Protein sequence of HRJDs used in this study, which derived from *Dugesia japonica*
545 (DjHRJDa/b, hereafter simply described as HRJDa/b). Conserved residues characteristic
546 of the JmjC domain are shown.

547 (C) Schematics of genetic experiments for whole body induction of HRJDs. The Gal4-
548 UAS system enables gene expression downstream of the UAS sequence, which is
549 regulated by the transcription factor Gal4 [15]. In this case, the ubiquitously active *Act5C*
550 promoter is used for Gal4 expression.

551 (D) Representative images of mature adults for whole body expression of HRJDs.

552 (E) Whole body induction of HRJDs did not change body weight of mature adults.

553 (F) Representative images of adult wings.

554 (G) Whole body induction of HRJDs did not change wing size.

555 (H) Representative images for adult heads.

556 (I) Whole body induction of HRJDs did not change eye size of adult flies.

557 N.S., not significant: P>0.05. One-way ANOVAs with post hoc Tukey test. *n* indicates

558 the number of flies examined. See also Fig. S1.

559

560 **Figure 2. HRJD expression impedes tissue regeneration in the developing wind disc**

561 (A) Schematics of genetic ablation of the wing disc. TNF ligand *eiger* was overexpressed

562 in the wing pouch for 40 hrs during the larval stage.

563 (B) Wing regeneration was assessed in the adult stage by checking the size of wing (0%:

564 no wing, 100%: intact wing).

565 (C) Line graph for wing regeneration. Expression of HRJDa/b increased the rate of low

566 regeneration (0% and 25%) at the expense of the rate of full regeneration (100%).

567 (D-E) Representative images for adult wings of *WP-QF>QUAS-HRJDa/b* flies under

568 homeostatic (non-regenerative) condition (D). The wing size is quantified in (E).

569 N.S., not significant: P>0.05, ***P ≤0.001. Chi-square test (C) and one-way ANOVAs

570 with post hoc Tukey test (E). *n* indicates the number of wings examined.

571

572 **Figure 3. HRJDs expression compromises regeneration in the adult midgut**

573 (A) Schematics of the *Drosophila* adult midgut. The adult midgut is a pseudostratified

574 epithelium, in which intestinal stem cells (ISCs) generate both absorptive enterocytes

575 (ECs) and secretory enteroendocrine cells (EEs) through progenitor cell enteroblasts

576 (EBs) and EE progenitor cells (EEPs).

577 (B) Experimental scheme for ISC/EB specific induction of HRJDs under the *esg-Gal4*

578 driver in the adult stage. Adult flies were transferred to 29°C at Day 3 to induce HRJD

579 expression.

580 (C-E) Survival curve during paraquat (C), DSS (D), and sucrose (E) feeding.

581 (F) Representative images for PH3 staining upon paraquat feeding.

582 (G) Quantification of PH3 positive cells in posterior midguts.

583 N.S., not significant: P>0.05, *P<0.05, **P≤0.01. Log-rank test. *n* indicates the number

584 of flies (C-E) and midguts (G). Scale bars: 50 μm. See also Fig. S2.

585

586 **Figure 4. Post-developmental HRJD expression in ISC lineages extends organismal**

587 **lifespan**

588 (A-D) Survival curve for organismal lifespan by sex. HRJDs are induced by *esg*^{ts}*-Gal4*

589 (A and B) and *Act5C-Gal4* (C and D). For temporal regulation of HRJD induction using

590 *tub-Gal80*^{ts} (A and B), adult flies were transferred to 29°C at Day 3.

591 N.S., not significant: P>0.05, *P<0.05, **P≤0.01, ***P≤0.001, Log-rank tests. *n*

592 indicates the number of flies. See also Fig. S3.

593

594 **Figure 5. HRJD expression in adult ISCs/EBs suppress age-related gut barrier**

595 **dysfunction**

596 (A) *esg*^{ts}-mediated HRJD induction decreased Smurf(+) ratio at Day 30. The

597 representative images of the Smurf phenotype (leakage of blue dye throughout whole

598 body) is shown on the left.

599 (B-C) HRJD expression in adult ISCs/EBs maintained junctional localization of Dlg

600 protein in ECs, which is quantified in (C).

601 (D-I) HRJD expression in adult ISCs/EBs maintained junctional localization of Tsp2A

602 (D), Mesh (E), and Ssk (F) in ECs, which is quantified in (G-I).

603 *P<0.05, ***P≤0.001, One-way ANOVAs with post hoc Tukey test. *n* indicates the

604 number of flies (A) and cells (C, G, H, I) examined. Scale bars: 50 μm.

605

606 **Figure 6. HRJD expression in adult ISCs/EBs improves stem cell functions in aged**

607 **midguts**

608 (A) Representative images for *esg-Gal4* positive cells in Day 30 midguts. HRJDs

609 suppressed mis-differentiation of esg^+ cells (cellular enlargement with polyploid large

610 nuclei).

611 (B) Quantification of nuclear size of *esg-Gal4* positive cells.

612 (C-D) Representative images (C) and quantification (D) of PH3 positive cells in Day 30

613 posterior midguts. Day 10 young guts are also quantified in (D).

614 (E) RT-qPCR of *Dl*, *nub*, and *pros* in Day 30 midguts. Expression levels were normalized

615 to those of GFP control.

616 (F) Schematic model for the impact of HRJDs on intestinal homeostasis. In old wildtype

617 midguts, ISCs over-proliferate, and their daughters fail to differentiate into ECs, resulting

618 in accumulation of mis-differentiated cells (*esg*+ large polyploid). HRJD expression in

619 adult ISCs/EBs further enhances ISC proliferation but suppresses mis-differentiation.

620 N.S., not significant: P>0.05, *P≤0.05, **P≤0.01, ***P≤0.001, one-way ANOVAs with

621 post hoc Tukey test. *n* indicates the number of cells (B), guts (D), and biological replicates

622 (E). Scale bars: 50 μm.

623

624 **Supplemental figure legends**

625

626 **Figure S1. Expression and localization of HRJD proteins**

627 (A) Western blots of S2 cell samples upon transfection of 3×FLAG-HRJDa/b. Anti-
628 FLAG was used to detect 3×FLAG-HRJDa/b proteins and anti-tubulin was used as the
629 loading control. Expected molecular weight: 52.0 kDa for 3×FLAG-HRJDa, 52.9 kDa
630 for 3×FLAG-HRJDb.

631 (B) Representative images of anti-FLAG staining using S2 cells transfected with
632 3×FLAG-HRJDa/b. Both HRJDa and HRJDb localized cytoplasm but not in nuclei. Scale
633 bar: 30 μm in wide-view images (left), 5 μm in magnified view images (yellow frames).

634 (C-D) Representative images of 3×FLAG-HRJDa/b localization in wing discs and adult
635 midguts. FLAG-tagged HRJDs were induced using *WP-Gal4* (C) or *esg-Gal4* (D). Scale
636 bars: 10 μm.

637

638 **Figure S2. Continuous expression of HRJDs throughout development hampers**
639 **intestinal regeneration**

640 (A-C) Organismal survival upon paraquat (A), DSS (B), and sucrose (C) feeding. Drug
641 feeding started at Day 7 after eclosion. HRJD induction using *esg-Gal4* throughout
642 development significantly decreased survival upon paraquat/DSS feeding.

643 (D) Expression of HRJDa using *esg-Gal4* decreased the number of PH3 positive cells in
644 the posterior midguts, while HRJDb did not change PH3 positive cell number.

645 N.S., not significant: $P>0.05$, $^{**}P\leq0.01$, $^{***}P\leq0.001$, one-way ANOVAs with post hoc

646 Tukey test. *n* indicates the number of flies (A-C) and guts (D).

647

648 **Figure S3. Organismal lifespan of flies expressing HRJDs in ECs and ISC/EBs**

649 (A-F) Survival curve for organismal lifespan by sex. HRJDs are induced by *NP1-Gal4*

650 (A and B), *NP1^{ts}-Gal4* (C and D), and *esg-Gal4* (E and F).

651 N.S., not significant: P>0.05, ***P≤0.001, Log-rank tests. *n* indicates the number of flies.

652

653

654 **Table S1. Detailed genotypes in each experiment**

Fig.	Panel	Genotype
Fig. 1	**D-I**	*w;; Act5C-Gal4 / +*
		w; UAS-GFP / +; Act5C-Gal4 / UAS-HRJDb
		w;; Act5C-Gal4 / UAS-HRJDa
		w;; Act5C-Gal4 / UAS-HRJDb
Fig. 2	**A-C**	*w; rn-Gal4, tub-Gal80ts, UAS-egr / +; WP-QF2 / +*
		w; rn-Gal4, tub-Gal80ts, UAS-egr / +; WP-QF2 / QUAS-HRJDa
		w; rn-Gal4, tub-Gal80ts, UAS-egr / +; WP-QF2 / QUAS-HRJDb
	D-E	*w;; WP-QF2 / +*
		w;; WP-QF2 / QUAS-HRJDa
		w;; WP-QF2 / QUAS-HRJDb
Fig. 3	**C-G**	*w; esg-Gal4, tub-Gal80ts / UAS-GFP*
		w; esg-Gal4, tub-Gal80ts / +; UAS-HRJDa / +
		w; esg-Gal4, tub-Gal80ts / +; UAS-HRJDb / +
Fig. 4	**A-B**	*w; esg-Gal4, tub-Gal80ts / UAS-GFP*
		w; esg-Gal4, tub-Gal80ts / +; UAS-HRJDa / +
		w; esg-Gal4, tub-Gal80ts / +; UAS-HRJDb / +
	C-D	*w; UAS-GFP / +; Act5C-Gal4 / +*
		w;; Act5C-Gal4 / UAS-HRJDa
		w;; Act5C-Gal4 / UAS-HRJDb
Fig. 5, 6	**All**	*w; esg-Gal4, tub-Gal80ts / UAS-GFP*
		w; esg-Gal4, tub-Gal80ts / +; UAS-HRJDa / +
		w; esg-Gal4, tub-Gal80ts / +; UAS-HRJDb / +
Fig. S1	**C**	*w;; WP-Gal4 / +*
		w;; WP-Gal4 / UAS-FLAG-HRJDa
		w;; WP-Gal4 / UAS-FLAG-HRJDb
	D	*w; esg-Gal4, tub-Gal80ts, UAS-GFP / +*
		w; esg-Gal4, tub-Gal80ts, UAS-GFP / +; UAS-FLAG-HRJDa / +
		w; esg-Gal4, tub-Gal80ts, UAS-GFP / +; UAS-FLAG-HRJDb / +
Fig. S2	**All**	*w; esg-Gal4 / UAS-GFP*

		w; esg-Gal4 / +; UAS-HRJDa / +
		w; esg-Gal4 / +; UAS-HRJDb / +
Fig. S3	**A-B**	*w; NP1-Gal4 / UAS-GFP*
		w; NP1-Gal4 / +; UAS-HRJDa / +
		w; NP1-Gal4 / +; UAS-HRJDb / +
	C-D	*w; NP1-Gal4, tub-Gal80ts / UAS-GFP*
		w; NP1-Gal4, tub-Gal80ts / +; UAS-HRJDa / +
		w; NP1-Gal4, tub-Gal80ts / +; UAS-HRJDb / +
	E-F	*w; esg-Gal4 / UAS-GFP*
		w; esg-Gal4 / +; UAS-HRJDa / +
		w; esg-Gal4 / +; UAS-HRJDb / +

References

1. Bely AE, Nyberg KG. Evolution of animal regeneration: re-emergence of a field. Trends Ecol Evol. 2010;25:161–70.

2. Poss KD. Advances in understanding tissue regenerative capacity and mechanisms in animals. Nat Rev Genet. 2010;11:710–22.

3. Tiozzo S, Copley RR. Reconsidering regeneration in metazoans: an evo-devo approach. Front Ecol Evol. 2015;3.

4. Bideau L, Kerner P, Hui J, Vervoort M, Gazave E. Animal regeneration in the era of transcriptomics. Cell Mol Life Sci. 2021;78:3941–56.

5. Fujita S, Kuranaga E, Nakajima Y. Regeneration Potential of Jellyfish: Cellular Mechanisms and Molecular Insights. Genes. 2021;12:758.

6. Piraino S, Boero F, Aeschbach B, Schmid V. Reversing the Life Cycle: Medusae Transforming into Polyps and Cell Transdifferentiation in *Turritopsis nutricula* (Cnidaria, Hydrozoa). Biol Bull. 1996;190:302–12.

7. Varley Á, Horkan HR, McMahon ET, Krasovec G, Frank U. Pluripotent, germ cell competent adult stem cells underlie cnidarian regenerative ability and clonal growth. Curr Biol. 2023;33:1883-1892.e3.

8. Gazave E, Röttinger E. 7th Euro Evo Devo meeting: Report on the “Evolution of regeneration in Metazoa” symposium. J Exp Zoolog B Mol Dev Evol. 2021;336:89–93.

676 9. Kumar A, Godwin JW, Gates PB, Garza-Garcia AA, Brockes JP. Molecular Basis for
677 the Nerve Dependence of Limb Regeneration in an Adult Vertebrate. Science.
678 2007;318:772–7.
679 10. Da Silva SM, Gates PB, Brockes JP. The Newt Ortholog of CD59 Is Implicated in
680 Proximodistal Identity during Amphibian Limb Regeneration. Dev Cell. 2002;3:547–
681 55.
682 11. Looso M, Preussner J, Sousounis K, Bruckskotten M, Michel CS, Lignelli E, et al.
683 A de novo assembly of the newt transcriptome combined with proteomic validation
684 identifies new protein families expressed during tissue regeneration. Genome Biol.
685 2013;14:R16.
686 12. Mehta AS, Deshpande P, Chimata AV, Tsonis PA, Singh A. Newt regeneration
687 genes regulate Wingless signaling to restore patterning in Drosophila eye. iScience.
688 2021;24:103166.
689 13. Cao P-L, Kumagai N, Inoue T, Agata K, Makino T. JmjC Domain-Encoding Genes
690 Are Conserved in Highly Regenerative Metazoans and Are Associated with Planarian
691 Whole-Body Regeneration. Genome Biol Evol. 2019;11:552–64.
692 14. Umesono Y, Tasaki J, Nishimura Y, Hrouda M, Kawaguchi E, Yazawa S, et al. The
693 molecular logic for planarian regeneration along the anterior–posterior axis. Nature.
694 2013;500:73–6.
695 15. Brand AH, Perrimon N. Targeted gene expression as a means of altering cell fates
696 and generating dominant phenotypes. Development. 1993;118:401–15.
697 16. Hariharan IK, Serras F. Imaginal disc regeneration takes flight. Curr Opin Cell Biol.
698 2017;48:10–6.
699 17. Smith-Bolton RK, Worley MI, Kanda H, Hariharan IK. Regenerative Growth in
700 Drosophila Imaginal Discs Is Regulated by Wingless and Myc. Dev Cell. 2009;16:797–
701 809.
702 18. Worley MI, Alexander LA, Hariharan IK. CtBP impedes JNK- and Upd/STAT-
703 driven cell fate misspecifications in regenerating Drosophila imaginal discs. eLife.
704 2018;7:e30391.
705 19. Potter CJ, Tasic B, Russler EV, Liang L, Luo L. The Q System: A Repressible
706 Binary System for Transgene Expression, Lineage Tracing, and Mosaic Analysis. Cell.
707 2010;141:536–48.
708 20. Riabinina O, Luginbuhl D, Marr E, Liu S, Wu MN, Luo L, et al. Improved and

709 expanded Q-system reagents for genetic manipulations. Nat Methods. 2015;12:219–22.
710 21. Nagai H, Miura M, Nakajima Y. Cellular mechanisms underlying adult tissue
711 plasticity in Drosophila. Fly (Austin). 2022;16:190–206.
712 22. Miguel-Aliaga I, Jasper H, Lemaitre B. Anatomy and Physiology of the Digestive
713 Tract of *Drosophila melanogaster*. Genetics. 2018;210:357–96.
714 23. Zhang P, Edgar BA. Insect Gut Regeneration. Cold Spring Harb Perspect Biol.
715 2021;:a040915.
716 24. Jasper H. Intestinal Stem Cell Aging: Origins and Interventions. Annu Rev Physiol.
717 2020;82:203–26.
718 25. Buchon N, Broderick NA, Chakrabarti S, Lemaitre B. Invasive and indigenous
719 microbiota impact intestinal stem cell activity through multiple pathways in *Drosophila*.
720 Genes Dev. 2009;23:2333–44.
721 26. Jiang H, Patel PH, Kohlmaier A, Grenley MO, McEwen DG, Edgar BA.
722 Cytokine/Jak/Stat Signaling Mediates Regeneration and Homeostasis in the Drosophila
723 Midgut. Cell. 2009;137:1343–55.
724 27. Biteau B, Hochmuth CE, Jasper H. JNK Activity in Somatic Stem Cells Causes
725 Loss of Tissue Homeostasis in the Aging Drosophila Gut. Cell Stem Cell. 2008;3:442–
726 55.
727 28. Amcheslavsky A, Jiang J, Ip YT. Tissue Damage-Induced Intestinal Stem Cell
728 Division in Drosophila. Cell Stem Cell. 2009;4:49–61.
729 29. Jiang H, Edgar BA. EGFR signaling regulates the proliferation of *Drosophila* adult
730 midgut progenitors. Development. 2009;136:483–93.
731 30. Houtz P, Bonfini A, Bing X, Buchon N. Recruitment of Adult Precursor Cells
732 Underlies Limited Repair of the Infected Larval Midgut in Drosophila. Cell Host
733 Microbe. 2019;26:412-425.e5.
734 31. Rera M, Bahadorani S, Cho J, Koehler CL, Ulgherait M, Hur JH, et al. Modulation
735 of Longevity and Tissue Homeostasis by the Drosophila PGC-1 Homolog. Cell Metab.
736 2011;14:623–34.
737 32. Thevaranjan N, Puchta A, Schulz C, Naidoo A, Szamosi JC, Verschoor CP, et al.
738 Age-Associated Microbial Dysbiosis Promotes Intestinal Permeability, Systemic
739 Inflammation, and Macrophage Dysfunction. Cell Host Microbe. 2017;21:455-466.e4.
740 33. Nagai H, Tatara H, Tanaka-Furuhashi K, Kurata S, Yano T. Homeostatic Regulation
741 of ROS-Triggered Hippo-Yki Pathway via Autophagic Clearance of Ref(2)P/p62 in the

742 Drosophila Intestine. Dev Cell. 2021;56:81-94.e10.
743 34. Egge N, Arneaud SLB, Wales P, Mihelakis M, McClendon J, Fonseca RS, et al.
744 Age-Onset Phosphorylation of a Minor Actin Variant Promotes Intestinal Barrier
745 Dysfunction. Dev Cell. 2019;51:587-601.e7.
746 35. Rera M, Clark RI, Walker DW. Intestinal barrier dysfunction links metabolic and
747 inflammatory markers of aging to death in Drosophila. Proc Natl Acad Sci.
748 2012;109:21528–33.
749 36. Resnik-Docampo M, Koehler CL, Clark RI, Schinaman JM, Sauer V, Wong DM, et
750 al. Tricellular junctions regulate intestinal stem cell behaviour to maintain homeostasis.
751 Nat Cell Biol. 2017;19:52–9.
752 37. Salazar AM, Resnik-Docampo M, Ulgherait M, Clark RI, Shirasu-Hiza M, Jones
753 DL, et al. Intestinal Snakeskin Limits Microbial Dysbiosis during Aging and Promotes
754 Longevity. iScience. 2018;9:229–43.
755 38. Izumi Y, Furuse K, Furuse M. Septate junctions regulate gut homeostasis through
756 regulation of stem cell proliferation and enterocyte behavior in *Drosophila*. J Cell Sci.
757 2019;:jcs.232108.
758 39. Chen H, Zheng X, Zheng Y. Age-Associated Loss of Lamin-B Leads to Systemic
759 Inflammation and Gut Hyperplasia. Cell. 2014;159:829–43.
760 40. Korzelius J, Naumann SK, Loza-Coll MA, Chan JS, Dutta D, Oberheim J, et al.
761 *Escargot* maintains stemness and suppresses differentiation in *Drosophila* intestinal
762 stem cells. EMBO J. 2014;33:2967–82.
763 41. Li Y, Pang Z, Huang H, Wang C, Cai T, Xi R. Transcription Factor Antagonism
764 Controls Enteroendocrine Cell Specification from Intestinal Stem Cells. Sci Rep.
765 2017;7:988.
766 42. Clark RI, Salazar A, Yamada R, Fitz-Gibbon S, Morselli M, Alcaraz J, et al.
767 Distinct Shifts in Microbiota Composition during Drosophila Aging Impair Intestinal
768 Function and Drive Mortality. Cell Rep. 2015;12:1656–67.
769 43. Wang L, Ryoo HD, Qi Y, Jasper H. PERK Limits Drosophila Lifespan by
770 Promoting Intestinal Stem Cell Proliferation in Response to ER Stress. PLOS Genet.
771 2015;11:e1005220.
772 44. Markolovic S, Leissing TM, Chowdhury R, Wilkins SE, Lu X, Schofield CJ.
773 Structure–function relationships of human JmjC oxygenases—demethylases versus
774 hydroxylases. Curr Opin Struct Biol. 2016;41:62–72.

775 45. Hsia DA, Tepper CG, Pochampalli MR, Hsia EYC, Izumiya C, Huerta SB, et al.
776 KDM8, a H3K36me2 histone demethylase that acts in the cyclin A1 coding region to
777 regulate cancer cell proliferation. Proc Natl Acad Sci. 2010;107:9671–6.
778 46. Shalaby NA, Sayed R, Zhang Q, Scoggin S, Eliazer S, Rothenfluh A, et al.
779 Systematic discovery of genetic modulation by Jumonji histone demethylases in
780 Drosophila. Sci Rep. 2017;7:5240.
781 47. Klose RJ, Kallin EM, Zhang Y. JmjC-domain-containing proteins and histone
782 demethylation. Nat Rev Genet. 2006;7:715–27.
783 48. Curtis BJ, Zraly CB, Marenda DR, Dingwall AK. Histone lysine demethylases
784 function as co-repressors of SWI/SNF remodeling activities during Drosophila wing
785 development. Dev Biol. 2011;350:534–47.
786 49. Zhu Z, Chen X, Guo A, Manzano T, Walsh PJ, Wills KM, et al. Mitotic
787 bookmarking by SWI/SNF subunits. Nature. 2023;618:180–7.
788 50. Nakajima Y. Mitotic spindle orientation in epithelial homeostasis and plasticity. J
789 Biochem (Tokyo). 2018;164:277–84.
790 51. Goulas S, Conder R, Knoblich JA. The Par Complex and Integrins Direct
791 Asymmetric Cell Division in Adult Intestinal Stem Cells. Cell Stem Cell. 2012;11:529–
792 40.
793 52. Hu DJ-K, Jasper H. Control of Intestinal Cell Fate by Dynamic Mitotic Spindle
794 Repositioning Influences Epithelial Homeostasis and Longevity. Cell Rep.
795 2019;28:2807-2823.e5.
796 53. Brunet A, Goodell MA, Rando TA. Ageing and rejuvenation of tissue stem cells and
797 their niches. Nat Rev Mol Cell Biol. 2023;24:45–62.
798 54. Campisi J, Kapahi P, Lithgow GJ, Melov S, Newman JC, Verdin E. From
799 discoveries in ageing research to therapeutics for healthy ageing. Nature.
800 2019;571:183–92.
801 55. Kashio S, Obata F, Zhang L, Katsuyama T, Chihara T, Miura M. Tissue
802 nonautonomous effects of fat body methionine metabolism on imaginal disc repair in
803 *Drosophila*. Proc Natl Acad Sci. 2016;113:1835–40.
804 56. González M, Martín-Ruíz I, Jiménez S, Pirone L, Barrio R, Sutherland JD.
805 Generation of stable Drosophila cell lines using multicistronic vectors. Sci Rep.
806 2011;1:75.
807 57. Izumi Y, Motoishi M, Furuse K, Furuse M. A tetraspanin regulates septate junction

formation in *Drosophila* midgut. J Cell Sci. 2016;:jcs.180448.
58. Izumi Y, Yanagihashi Y, Furuse M. A novel protein complex, mesh-ssk, is required for septate junction formation in *drosophila* midgut. J Cell Sci. 2012;:jcs.112243.
59. Nakajima Y. Analysis of Epithelial Architecture and Planar Spindle Orientation in the Drosophila Wing Disc. In: Turksen K, editor. Stem Cell Renewal and Cell-Cell Communication. New York, NY: Springer US; 2020. p. 51–62.
60. Nakajima Y, Lee ZT, McKinney SA, Swanson SK, Florens L, Gibson MC. Junctional tumor suppressors interact with 14-3-3 proteins to control planar spindle alignment. J Cell Biol. 2019;218:1824–38.

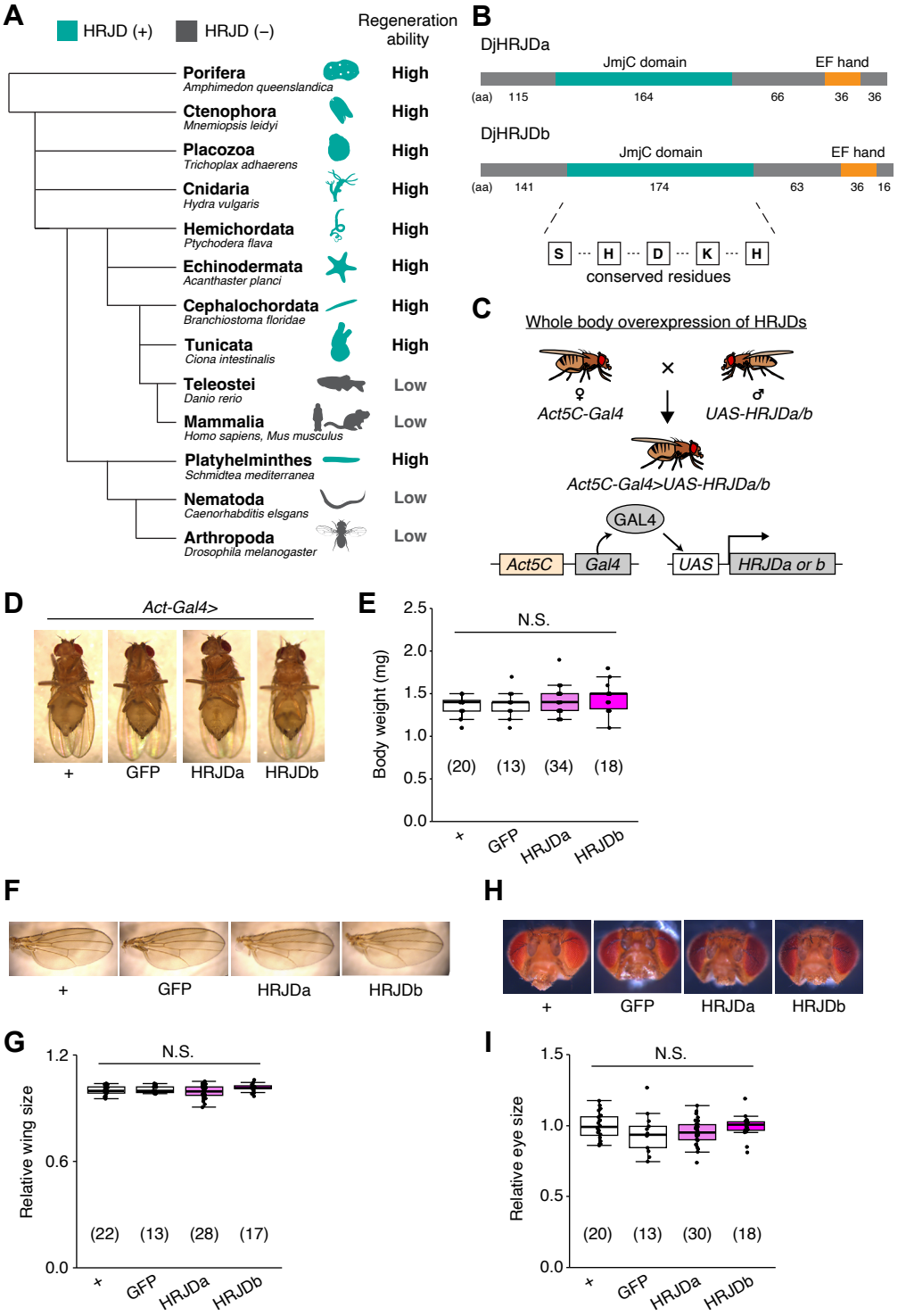
A
HRJD (+)
HRJD (–)
Regeneration ability
Porifera
Amphimedon queenslandica
High
Ctenophora
Mnemiopsis leidyi
High
Placozoa
Trichoplax adhaerens
High
Cnidaria
Hydra vulgaris
High
Hemichordata
Ptychodera flava
High
Echinodermata
Acanthaster planci
High
Cephalochordata
Branchiostoma floridae
High
Tunicata
Ciona intestinalis
High
Teleostei
Danio rerio
Low
Mammalia
Homo sapiens, Mus musculus
Low
Platyhelminthes
Schmidtea mediterranea
High
Nematoda
Caenorhabditis elsgans
Low
Arthropoda
Drosophila melanogaster
Low
B
DjHRJDa
JmjC domain
EF hand
(aa) 115 164 66 36 36
DjHRJDb
JmjC domain
EF hand
(aa) 141 174 63 36 16
S H D K H
conserved residues
C
Whole body overexpression of HRJDs
Act5C-Gal4
UAS-HRJDa/b
Act5C-Gal4>UAS-HRJDa/b
GAL4
Act5C
Gal4
UAS
HRJDa or b
D
Act-Gal4>
+
GFP
HRJDa
HRJDb
E
N.S.
Body weight (mg)
2.5
2.0
1.5
1.0
0.5
0.0
(20) (13) (34) (18)
+
GFP
HRJDa
HRJDb
F
+
GFP
HRJDa
HRJDb
H
+
GFP
HRJDa
HRJDb
G
N.S.
Relative wing size
1.2
0.6
0.0
(22) (13) (28) (17)
+
GFP
HRJDa
HRJDb
I
N.S.
Relative eye size
1.5
1.0
0.5
0.0
(20) (13) (30) (18)
+
GFP
HRJDa
HRJDb

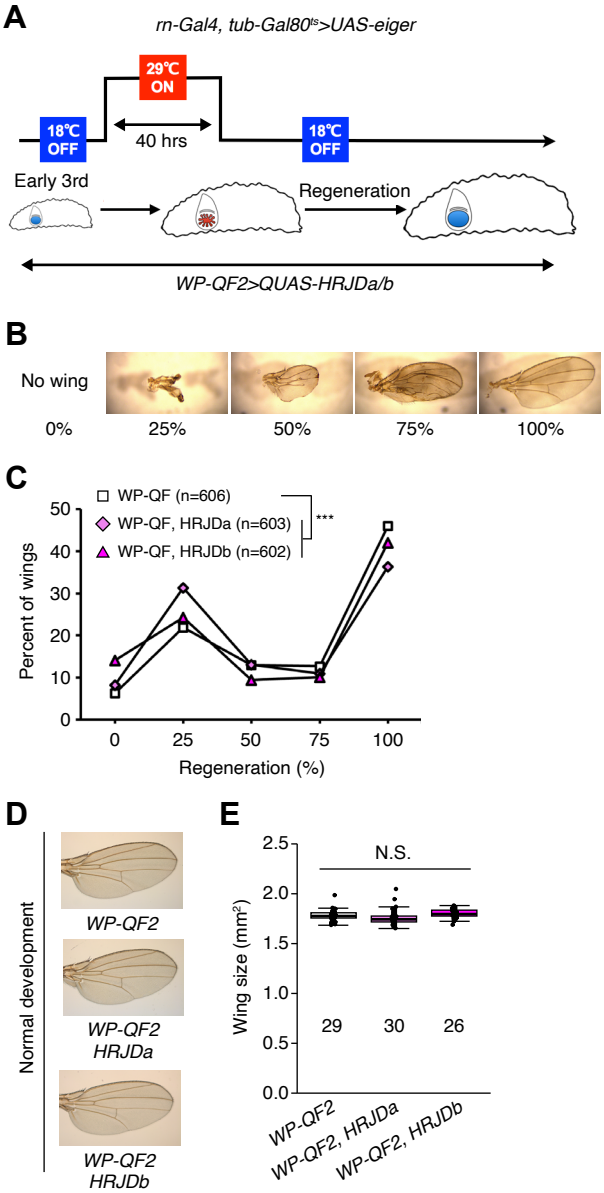
A
rn-Gal4, tub-Gal80ts>UAS-eiger
29°C ON
18°C OFF
40 hrs
18°C OFF
Early 3rd
Regeneration
WP-QF2>QUAS-HRJDa/b
B
No wing
0%
25%
50%
75%
100%
C
WP-QF (n=606)
WP-QF, HRJDa (n=603)
WP-QF, HRJDb (n=602)
***
Percent of wings
Regeneration (%)
D
Normal development
WP-QF2
WP-QF2 HRJDa
WP-QF2 HRJDb
E
N.S.
Wing size (mm²)
29
30
26
WP-QF2
WP-QF2, HRJDa
WP-QF2, HRJDb

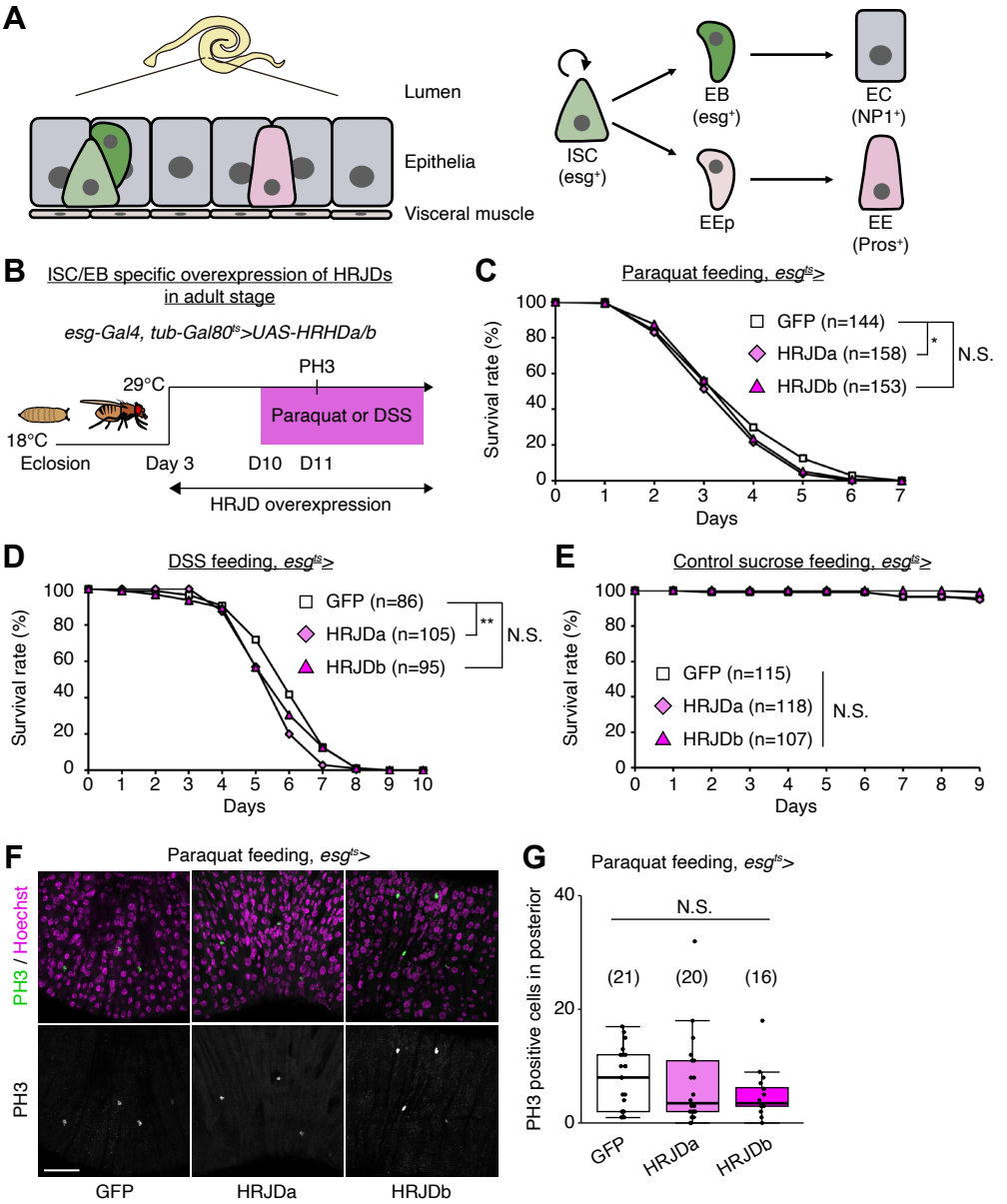
A
Lumen
Epithelia
Visceral muscle
ISC
(esg+)
EB
(esg+)
EC
(NP1+)
EEp
EE
(Pros+)
B
ISC/EB specific overexpression of HRJDs in adult stage
esg-Gal4, tub-Gal80ts>UAS-HRHDa/b
29°C
18°C
Eclosion
Day 3
PH3
Paraquat or DSS
D10
D11
HRJD overexpression
C
Paraquat feeding, esgts>
Survival rate (%)
Days
GFP (n=144)
HRJDa (n=158)
HRJDb (n=153)
*
N.S.
D
DSS feeding, esgts>
GFP (n=86)
HRJDa (n=105)
HRJDb (n=95)
**
N.S.
E
Control sucrose feeding, esgts>
GFP (n=115)
HRJDa (n=118)
HRJDb (n=107)
N.S.
F
Paraquat feeding, esgts>
PH3 / Hoechst
PH3
GFP
HRJDa
HRJDb
G
Paraquat feeding, esgts>
PH3 positive cells in posterior
N.S.
(21)
(20)
(16)
GFP
HRJDa
HRJDb

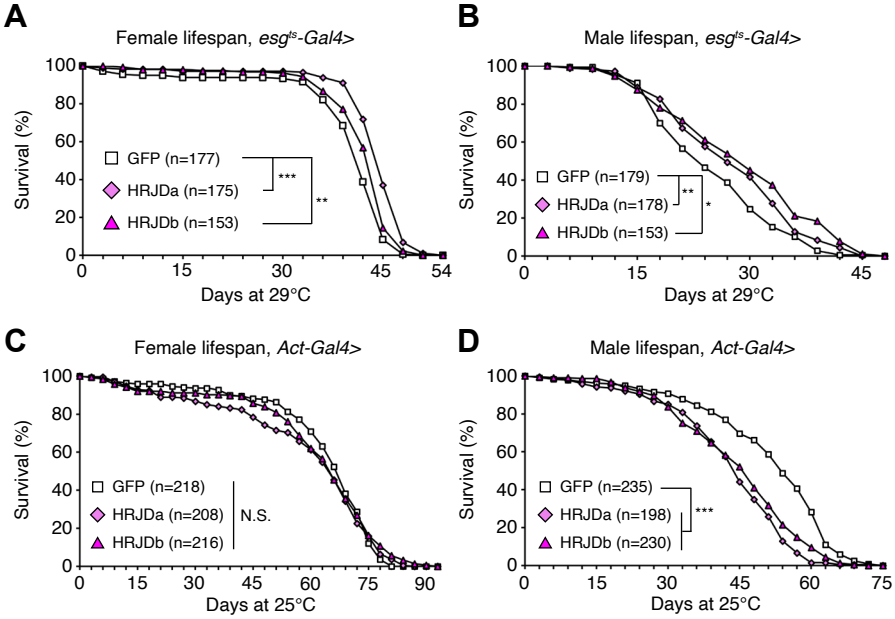
A
Female lifespan, esg^ts-Gal4>
Survival (%)
Days at 29°C
GFP (n=177)
HRJDa (n=175)
HRJDb (n=153)
***
**
B
Male lifespan, esg^ts-Gal4>
Survival (%)
Days at 29°C
GFP (n=179)
HRJDa (n=178)
HRJDb (n=153)
**
*
C
Female lifespan, Act-Gal4>
Survival (%)
Days at 25°C
GFP (n=218)
HRJDa (n=208)
HRJDb (n=216)
N.S.
D
Male lifespan, Act-Gal4>
Survival (%)
Days at 25°C
GFP (n=235)
HRJDa (n=198)
HRJDb (n=230)
***

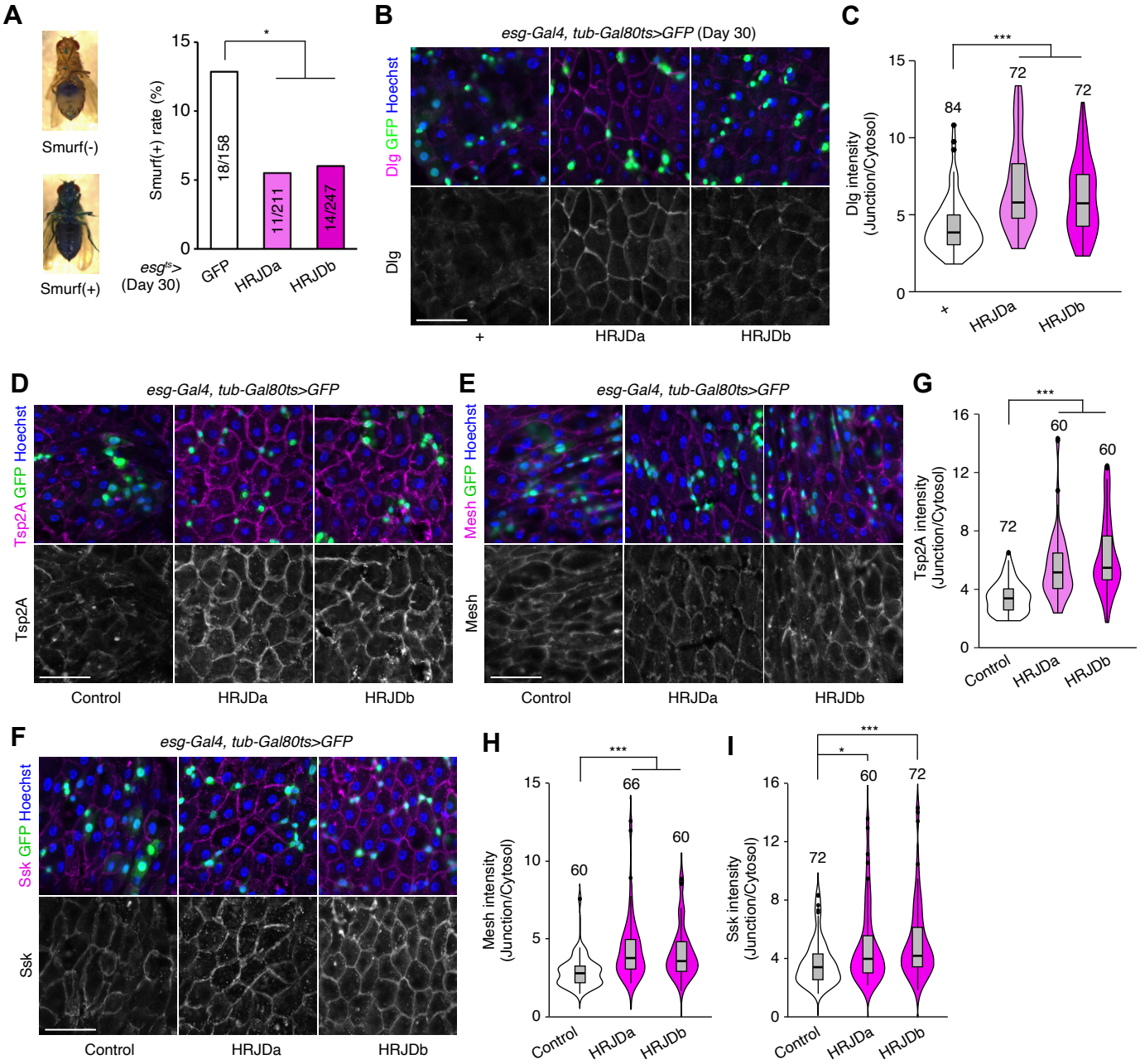
A
Smurf(-)
Smurf(+)
Smurf(+) rate (%)
18/158
11/211
14/247
esg^ts> (Day 30)
GFP
HRJDa
HRJDb
B
esg-Gal4, tub-Gal80ts>GFP (Day 30)
Dlg GFP Hoechst
Dlg
+
HRJDa
HRJDb
C
Dlg intensity (Junction/Cytosol)
84
72
72
D
esg-Gal4, tub-Gal80ts>GFP
Tsp2A GFP Hoechst
Tsp2A
Control
HRJDa
HRJDb
E
esg-Gal4, tub-Gal80ts>GFP
Mesh GFP Hoechst
Mesh
Control
HRJDa
HRJDb
G
Tsp2A intensity (Junction/Cytosol)
72
60
60
F
esg-Gal4, tub-Gal80ts>GFP
Ssk GFP Hoechst
Ssk
Control
HRJDa
HRJDb
H
Mesh intensity (Junction/Cytosol)
60
66
60
I
Ssk intensity (Junction/Cytosol)
72
60
72

Figure 6

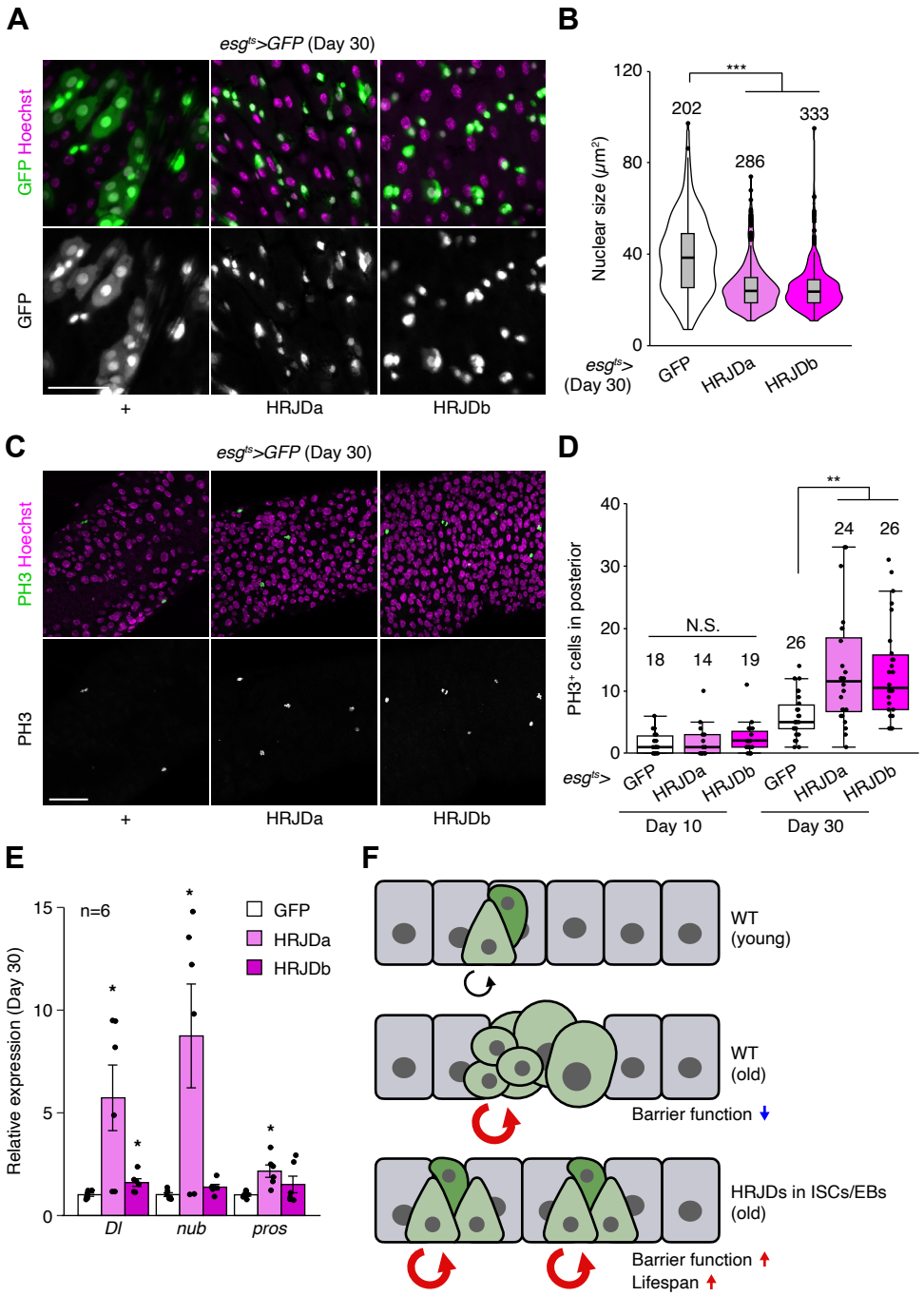
A
esg^ts>GFP (Day 30)
GFP Hoechst
GFP
+
HRJDa
HRJDb
B
Nuclear size (μm²)
120
80
40
0
***
202
286
333
esg^ts> (Day 30)
GFP
HRJDa
HRJDb
C
esg^ts>GFP (Day 30)
PH3 Hoechst
PH3
+
HRJDa
HRJDb
D
PH3⁺ cells in posterior
40
30
20
10
0
**
N.S.
18
14
19
26
24
26
esg^ts>
GFP
HRJDa
HRJDb
GFP
HRJDa
HRJDb
Day 10
Day 30
E
Relative expression (Day 30)
15
10
5
0
n=6
GFP
HRJDa
HRJDb
Dl
nub
pros
F
WT (young)
WT (old)
Barrier function ↓
HRJDs in ISCs/EBs (old)
Barrier function ↑
Lifespan ↑